Available online at www.sciencedirect.com
SCIENCE DIRECT®
Mendeleev Commun., 2007, **17**, 268–270
Mendeleev Communications

An XPS study of the synergetic effect of gold and nickel supported on SiO_2 in the catalytic isomerization of allylbenzene

Alexander Yu. Vasil'kov,*[a] Sergey A. Nikolaev,[b] Vladimir V. Smirnov,[b] Alexander V. Naumkin,[a] Ilija O. Volkov[a] and Vladislav L. Podshibikhin[a]

[a] *A. N. Nesmeyanov Institute of Organoelement Compounds, Russian Academy of Sciences, 119991 Moscow, Russian Federation. Fax: +7 495 135 5080; e-mail: alexvas@ineos.ac.ru*
[b] *Department of Chemistry, M. V. Lomonosov Moscow State University, 119992 Moscow, Russian Federation*

DOI: 10.1016/j.mencom.2007.09.006

A synergetic effect and catalytic activity in allylbenzene isomerization have been found for the Au–Ni/SiO_2 system prepared by metal-vapour synthesis.

The high catalytic activity and selectivity of gold nanoparticles are attractive.[1] The metal-vapour synthesis (MVS) is widely used for the preparation of colloidal solutions,[2] polymers[3] and inorganic nanomaterials[4] containing Au nanoparticles. For example,[5] gold-containing nanoparticles obtained by MVS and supported on SiO_2 and γ-Al_2O_3 manifested a high catalytic activity in CCl_4 addition to multiple bonds.

The aim of this work was to study the catalytic activity of a gold-containing nanocomposite towards the allylbenzene isomerization to *trans*- and *cis*-methylstyrene.

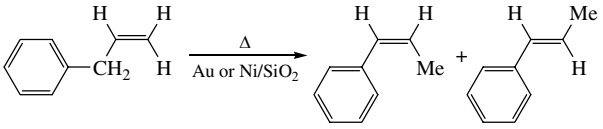

The catalysis of the process with gold-containing nanocomposites is characterised by a strong size effect and synergism of the catalytic activity in the case of systems containining gold and nickel simultaneously.

For the catalyst preparation, metals of 99.8–99.9% purity were used. A tungsten rod with a diameter of 1.5–2 mm (99.98% purity) was used as a metal evaporator. Toluene, triethylamine and allylbenzene (Aldrich) were dried over CaH_2 or Na and used as-dephlegmated. Fine silica powder (Aldrich, 500 m^2 g^{-1}) was used as a substrate for supporting Au-containing nanoparticles. Before deposition, the substrates were activated at 10^{-2} Torr and 300 °C for 6 h. All organic reactants were outgassed by several consecutive freeze–thaw cycles at at least 10^{-2} Torr just before their utilization in the MVS.

Vapours of one or two metals were deposited on a reactor surface cooled with liquid nitrogen simultaneously with Et_3N or PhMe at 10^{-4} Torr. At the end of the synthesis, the cooling was stopped, the reactor was filled with argon and the suspension of the co-condensate was pressed out from the reactor into a Schlenk bulb containing SiO_2 under vacuum. The excessive suspension was removed, and the as-prepared composite was dried at 10^{-2} Torr and 100 °C. Supported systems were prepared by the impregnation of the activated substrate with mono- or bimetallic organosols, which were prepared by MVS using a stationary set-up with a 5 dm^3 glass reactor.[6] The metal content of the samples was determined by atomic adsorption spectrometry (AAS) on a Hitachi 180-80 instrument. The metal was washed off the support with a solution of HCl–HNO_3 (4:1). The sensitivity of this method was 5×10^{-6}–5×10^{-5} g dm^{-3}.

The dispersion of supported particles was estimated by X-ray analysis using an approach described elsewhere.[7] All the preparation steps were done under argon purified by the usual Schlenk technique.

The XPS spectra were recorded on a Kratos XSAM-800 spectrometer using MgKα radiation (90 W) at about 10^{-8} Torr. Gold and nickel foils used as reference samples were cleaned by Ar^+ ion bombardment (partial pressure of 5×10^{-5} Torr) at a kinetic energy of 2 keV at an incidence angle of 45° in an ultrahigh vacuum (below 10^{-8} Torr). The XPS spectra were background subtracted (assuming linear and Shirley background due to the secondary electrons for the insulating catalysts and metal foils, respectively) and fitted with Gaussian line profiles.

The Si 2*p* (103.9 eV) peak for the SiO_2 substrate was used for the charge compensation and calibration of binding energies. The quantitative analysis was based on the atomic sensitivity factors.[8] The samples were placed into the spectrometer onto a Ti sample holder and catalytical reactor in atmospheric environment.

The catalytic activity towards the allylbenzene isomerization A (mole of product mole of $metal^{-1}$ h^{-1}) was measured by usual experiments: 0.1 g catalyst at metal content in the sample of 10^{-5}–10^{-6} mol, 7.5×10^{-4} mol of allylbenzene, 170 °C. The as-measured reaction rate was normalised to the metal content at a surface of gold nanoparticles, which was estimated using relations obtained in hemisphere approximation of particle shape.[9,10]

Catalytic experiments were performed in glass ampoules under vacuum conditions with intense agitation, under conditions of the kinetic control of the reaction process. The products were analysed by gas chromatography and chromatography-mass-spectrometry.

PhMe and Et_3N were used in MVS for the preparation of Au, Fe, Co and Ni organosoles.[5–7] The utilization of Et_3N is preferable for the preparation of the supported Au system since a particle size distribution with a maximum at about 3 nm can be obtained in this case. The utilization of an Au–PhMe suspension gives rise to the formation of larger particles of size 20–40 nm. For the Ni–Et_3N system, a broad particle size distribution from 15 to 95 nm with a maximum at 50 nm was measured.

The supported systems based on gold sols in toluene containing particles with the average size $d(Au_n)_{av} > 30$ nm are inactive in allylbenzene isomerization. A decrease in the gold particle size down to 2–3 nm causes a sharp increase in the catalytic activity. Data on the catalytic activity of nanocomposites **1**–**5**, their compositions and properties are presented in Table 1.

Table 1 Characteristics and properties of nanocomposites **1**–**5**.

Sample		Au (wt%)	Ni (wt%)	Au/ Ni_{bulk}	Au/ Ni_{surf}	Surface composition	Average size/nm	Catalytic activity/ mol $mol^{-1}_{Au_{surf}}$ h^{-1}	E_b, Ni $2p_{3/2}$/ eV	E_b, Ni $2p_{3/2}$ sat/eV	E_b, Au $4f_{7/2}$/eV (FWHM/ eV)	E_b, Au $4f_{5/2}$/eV (FWHM/ eV)	E_b, Ni $2p_{3/2}$ – Au $4f_{7/2}$/ eV
Au–Ni/SiO_2	**1**	0.14	0.10	0.4	0.3	$SiO_{2.8}Au_{0.11}Ni_{0.4}C_2$	2.3[a]	5580	856.0	861.6	84.3 (2.1)	87.9 (2.5)	771.7
	2	0.49	0.16	0.9	1.0	$SiO_{2.1}Au_{0.2}Ni_{0.2}O_{0.8}C_{1.2}$	2.9[a]	4620	856.7	862.2	84.2 (2.2)	87.8 (2.5)	772.5
	3	0.45	0.46	0.3	0.3	$SiO_{2.8}Au_{0.2}Ni_{0.7}C_{1.6}$	3.0[a]	242	856.9	862.7	84.0 (2.5)	87.6 (2.7)	772.9
Ni/SiO_2	**4**	—	0.30			$SiO_{2.3}Ni_{0.1}C_{1.3}$	50	0	855.9	861.5			
Au/SiO_2	**5**	0.21	—			$SiO_{2.0}Au_{0.01}C_{0.5}$	2.1	108			84.0 (2.2)	87.6 (2.2)	

[a]The first (sharp) maximum of bimodal distribution. The second (broad) maximum is about 45 nm.

In order to understand the nature of the synergetic influence of Ni on the Au + Ni system, the active surface of nanocomposites **1**–**5** was studied by XPS. Figure 1 shows the Ni $2p_{3/2}$ and Au $4f_{7/2}$ core-level lines of mono- and bimetallic samples, which differ in the relative Au and Ni atomic concentrations, whereas the quantitative surface analysis data and Ni and Au core-level binding energies (E_b) are summarized in Table 1. A comparison of the Au/Ni bulk and surface concentration ratios shows that they are close to each other, *i.e.*, no preferential deposition or inclusion inside the sample of one of the metals occurs. Thus, through the XPS sampling depth, no inhomogeneous metal distribution was detected.

The comparative analysis of the E_b of Au $4f_{7/2}$ lines allowed us to suggest a correlation between the XPS data and the catalytic activity. The higher the catalytic activity of a sample, the higher the E_b of Au $4f_{7/2}$ and the smaller the peak width. A decrease in the Au $4f_{7/2}$ peak width (Table 1) may be due to a decrease in the concentration of catalytically inactive states.

The difference of the Ni $2p_{3/2}$ and Au $4f_{7/2}$ binding energies (ΔE_b), which is 771.7, 772.5 or 772.9 eV in **1**, **2** and **3**, respectively, may be used as a parameter characterising interaction between Au and Ni. The parameter ΔE_b, as well as E_b(Au $4f_{7/2}$), correlates with the catalytic activity. The value of 771.7 eV corresponds to the highest catalytic activity. The interaction between these metals induces a positive binding energy shift of the core level of one metal and a negative shift of the other, which indicates alloy formation. It was shown that ΔE_b of $Au_{0.5}Ni_{0.5}$ cluster was 768.35 eV.[11] Such distinct differences in $Au_{0.5}Ni_{0.5}$ cluster's and **1**–**3** ΔE_b values are related to the absence of 'pure' interaction between Au and Ni in **1**–**3**, due to the presence of oxygen and carbon in the substrate.

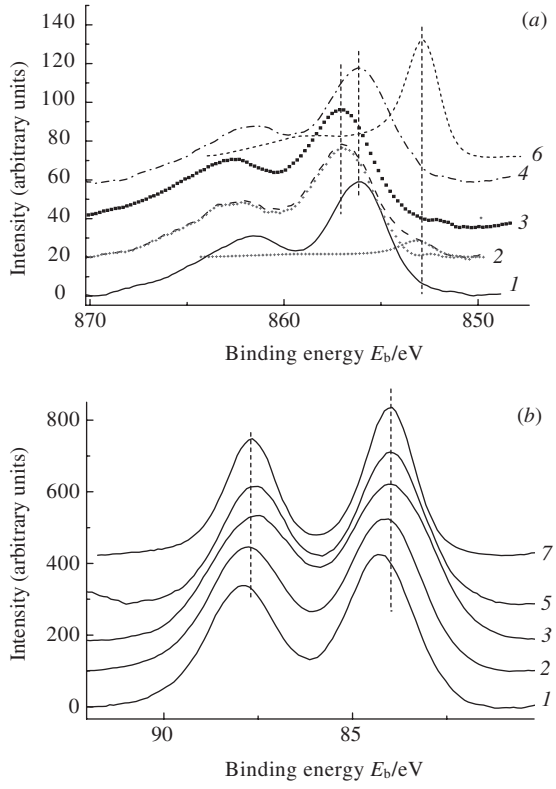

Figure 1 (*a*) Ni $2p_{3/2}$ and (*b*) Au $4f$ core level photoelectron spectra of (*1*)–(*3*) Au–Ni/SiO_2 **1**–**3**, (*4*) Ni/SiO_2 **4**, (*5*) Au/SiO_2 **5**, (*6*) Ni foil and (*7*) Au foil. The Ni $2p_{3/2}$ spectrum (*2*) fitted by metal and oxide states.

We consider the samples as a set of subsequent compositional transformation: **4** → **1** → **2** → **3**. A comparison of spectral features of **4** and published data[12–21] show that the main state of nickel is NiO. At least, the interaction of active metal with the substrate surface results in the oxidation of the surface layer of nickel nanoclusters.

The addition of Au (sample **1**) does not change the nickel chemical state: a typical spectrum of Ni^{2+} is observed. The Ni $2p_{3/2}$ binding energy and the line shapes in samples **4** and **1** are similar. However, the Au $4f_{7/2}$ peak in the spectrum of **1** shifts to higher energy by 0.3 eV relative to that of **5** that may be an evidence of the Ni influence on a change of the interactions between Au and the substrate, due to the formation of structures like Au/NiO/SiO_2, NiO/Au/SiO_2 or $AuNi_xO_y/SiO_2$. Change of relative and absolute metal contents will cause a redistribution of weight coefficients of the structures mentioned above and thus appear in photoelectron spectra.

The Au content increase in **2** in comparison with **1** induces essential changes of Ni spectral features. The Ni $2p_{3/2}$ peak shifts to a high binding energy and a new state appearing at 853.1 eV evidences the Ni^0 state, although Ni^{2+} remains the main state, as in **1**. The Ni^0 state is observed in the valence band spectrum of sample **2**. The valence band spectra show that variable amounts of Ni^0 are present in all the samples, excluding topmost nanocluster layers. It is related to the fact that inelastic mean free path of the valence electrons is about twice longer than that of the Ni $2p$ electrons.[22] An increase in the absolute metal content in **3** in comparison with **1** at a constant Au/Ni ratio induces the Ni $2p_{3/2}$ peak shift by 1.2 eV and an increase in the Au $4f_{7/2}$ full width at half maximum value by 0.4 eV. In this case, the Au $4f_{7/2}$ line broadening is very large and the Au spectrum includes all the states mentioned above. At the same time, there is a state with a binding energy less than that measured in **1**.

The fact of the mutual influence of Au and Ni in bimetallic catalyst on their spectral features manifests that the electronic properties of the components essentially change upon the formation of the bimetallic nanocomposites. The Ni $2p_{3/2}$ and Au $4f_{7/2}$ electron binding energies of some Au–Ni quasialloys were measured.[11] By comparing their values with those of **1**–**4**, one may conclude that the main Ni state is Ni^{2+}. The oxide shell prevents a direct contact between Au and Ni. The positive role of Ni expressed in the increase of the catalytic activity may be due to the limitation of Au contacts with the substrate, so as nickel and its oxides form an interface between SiO_2 and Au particles.

The appearance of the Ni^0 state in the the gold-rich samples is due to gold shielding of nickel nanoparticles, which prevents

contact of pure Ni with the surface during the formation of the catalyst. The influence of a hydrocarbon shell formed during the interaction of Et_3N with metal nanoparticles in MVS should also be taken into account. Such a process follows because of a high carbon content of a surface layer (Table 1) and high reactivity of nanoparticles. It may result in an increase in the Au $4f_{7/2}$ line width in sample **3**, which is the richest in terms of metal content and surface carbon. A similar change in the Au 4*f* line shape was observed previously[23] and interpreted as the formation of a hydrocarbon shell around the Au cluster.

This work was supported by the Russian Foundation for Basic Research (grant nos. 05-03-33065 and 06-03-33131).

References

1 R. Meyer, C. Lemire, Sh. K. Shaikhutdinov and H.-J. Freund, *Gold Bull.*, 2004, **37**, 72.
2 S.-T. Lin, M. T. Franklin and K. J. Klabunde, *Langmuir*, 1986, **2**, 259.
3 K. J. Klabunde, J. Habdas and G. Cardenas-Trivino, *Chem. Mater.*, 1989, **1**, 481.
4 B. L. V. Prasad, S. I. Stoeva, C. M. Sorensen, V. Zaikovski and K. J. Klabunde, *J. Am. Chem. Soc.*, 2003, **125**, 10488.
5 S. A. Nikolaev, A. Yu. Vasil'kov, V. V. Smirnov and L. A. Tjurina, *Kinet. Katal.*, 2005, **46**, 915 [*Kinet. Catal.* (*Engl. Transl.*), 2005, **46**, 867].
6 A. Yu. Vasil'kov, A. Yu. Olenin, E. F. Titova and V. A. Sergeev, *J. Colloid Interface Sci.*, 1995, **169**, 369.
7 V. V. Smirnov, S. N. Lanin, A. Yu. Vasil'kov, S. A. Nikolaev, G. P. Murav'eva, L. A. Tjurina and E. V. Vlasenko, *Izv. Akad. Nauk, Ser. Khim.*, 2005, 2215 (*Russ. Chem. Bull., Int. Ed.*, 2005, **54**, 2286).
8 A. V. Naumkin, I. O. Volkov, D. R. Tur and A. J. Pertsin, *Vysokomol. Soedin.,*2002, **44**, 877 [*Polym. Sci., Ser. B* (*Engl. Transl.*), 2002, **44**, 139].
9 V. I. Bukhtiyarov and M. G. Slin'ko, *Usp. Khim.*, 2001, **70**, 167 (*Russ. Chem. Rev.*, 2001, **70**, 147).
10 C. Mohr, H. Hofmeister and J. Radnik, *J. Catal.*, 2002, **213**, 86.
11 J. L. Rousset, F. J. Cadete Santos Aires, B. R. Sekhar, P. Merlinon, B. Prevel and M. Pellarin, *J. Phys. Chem. B*, 2000, **104**, 5430.
12 C. D. Wagner, A. V. Naumkin, A. Kraut-Vass, J. W. Allison, C. J. Powell and J. R. Rumble Jr., *NIST Standard Reference Database 20, Version 3.4*, 2003 (Web Version, http://srdata.nist.gov/xps/).
13 A. C. Miller and G. W. Simmons, *Surf. Sci. Spectra*, 1993, **1**, 312.
14 A. N. Mansour, *Surf. Sci. Spectra*, 1993, **3**, 221.
15 J. Arenas-Alattore, M. Avalos-Borja and G. Diaz, *Appl. Surf. Sci.*, 2002, **189**, 7.
16 A. N. Mansour and C. A. Melendres, *Surf. Sci. Spectra*, 1996, **3**, 231.
17 A. N. Mansour and C. A. Melendres, *Surf. Sci. Spectra*, 1996, **3**, 263.
18 A. N. Mansour and C. A. Melendres, *Surf. Sci. Spectra*, 1996, **3**, 247.
19 A. N. Mansour and C. A. Melendres, *Surf. Sci. Spectra*, 1996, **3**, 255.
20 A. N. Mansour, *Surf. Sci. Spectra*, 1996, **3**, 239.
21 A. N. Mansour and C. A. Melendres, *Surf. Sci. Spectra*, 1996, **3**, 271.
22 J. Powell and A. Jablonski, *NIST Electron Inelastic-Mean-Free-Path Database,Version 1.1*, National Institute of Standards and Technology, Gaithersburg, MD, 2000.
23 B. J. Tan, P. M. A. Sherwood and K. J. Klabunde, *Langmuir*, 1990, **6**, 106.

Received: 19th February 2007; Com. 07/2876